

MODEL COMPRESSION FOR DNN-BASED TEXT-INDEPENDENT SPEAKER VERIFICATION USING WEIGHT QUANTIZATION

Jingyu Li¹, Zhaoyang Zhang¹, Jiong Wang², Tan Lee¹

¹Department of Electronic Engineering, The Chinese University of Hong Kong, Hong Kong

²School of Science and Engineering, The Chinese University of Hong Kong, Shenzhen, China

ABSTRACT

DNN-based models achieve high performance in the speaker verification (SV) task with substantial computation costs. The model size is an essential concern in applying models on resource-constrained devices, while model compression for SV models has not been studied extensively in previous works. Weight quantization is exploited to compress DNN-based speaker embedding extraction models in this paper. Uniform and Powers-of-Two quantization are utilized in the experiments. The results on VoxCeleb show that the weight quantization can decrease the size of ECAPA-TDNN and ResNet by 4 times with insignificant performance decline. The quantized 4-bit ResNet achieves similar performance to the original model with an 8 times smaller size. We empirically show that the performance of ECAPA-TDNN is more sensitive than ResNet to quantization due to the difference in weight distribution. The experiments on CN-Celeb also demonstrate that quantized models are robust for SV in the language mismatch scenario.

Index Terms— text-independent speaker verification, weight quantization, model compression, weight distribution analysis

1. INTRODUCTION

Speech signals carry unique characteristics of the speaker, making speaker verification (SV) an option for biometric authentication [1, 2]. Automatic SV systems are constructed to determine whether the input utterances are given by the claimed speaker [3, 4]. GMM-UBM [5, 6] and I-vector [7] were dominant in this task. With the development of deep neural networks (DNN) in recent years, DNN-based models are now widely used in SV systems. DNN models are utilized to extract speaker embedding from the input utterance. With great learning ability, the state-of-the-art DNN-based models have shown much superior performance to conventional methods [8–10]. However, the performance is improved at the expense of high computation complexity.

A heavy burden of model computation could lead to difficulties in real-life model deployment. Applying models on local devices [11], e.g., smartphones, could be expected. Compared with online processing, i.e., cloud computation, offline computation has several advantages: (a) the data can be processed without the Internet, which avoids the transmission delay, (b) users' information is not exposed outside the device, which increases the safety of biometric privacy information. The resource on a local device is limited, and hence the model size is an essential concern in deploying a DNN model for applications.

To address the resource-constrained model computation issue, various model compression methods, like pruning [12, 13] and knowledge distillation [14], have been intensely studied in different tasks. The idea of model compression is to compress an existing

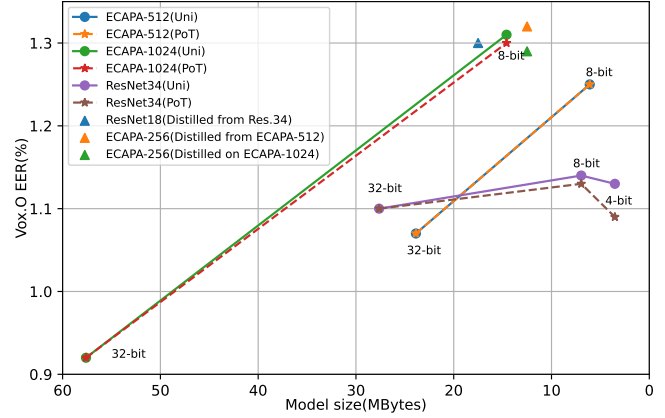


Fig. 1. Model Size vs. Vox1.O EER, lower is better. Uni stands for uniform quantization, and PoT stands for Powers-of-Two. The quantization bitwidth is annotated alongside the node. The distillation loss used here is \mathcal{L}_2 , applied on the speaker embedding level.

well-performed large-size model into a smaller size. To the best of our knowledge, the model compression for DNN-based SV systems is not studied in previous works. Weight quantization [15] is exploited to decrease the size of DNN-based speaker embedding extraction models in this paper. The data type used in current popular deep learning libraries is 32 bits, e.g., PyTorch [16] and TensorFlow [17]. The basic operation of quantization is mapping the full bitwidth model weights into data with lower bitwidth representation, e.g., 32→8 bits. The lower-bitwidth weights require a smaller model size. The model with low bitwidth can also be processed faster than the full-precision model. The model performance is affected dramatically by the error between the quantized weights and the original weights. Different methods [18, 19] are proposed for better reducing the quantization error. Two widely-used quantization methods are exploited in this paper: learnable uniform quantization [20] and Powers-of-Two quantization [21]. They are friendly for both software and hardware implementations.

The experiments are conducted on the VoxCeleb datasets [8, 22, 23]. ResNet [24] and ECAPA-TDNN [9] are utilized for speaker embedding extraction. Quantization shows different impacts on different types of model structures. Proper utilization of quantization compresses the model size by around 4 times, with a slight decrease in the performance. The models compressed by quantization outperform the models from distillation in our experiments, as shown in Fig. 1. We analyze the results of the compressed models to give some empirical guidelines on the quantization methods of SV models. The generalization ability of the quantized model is evaluated

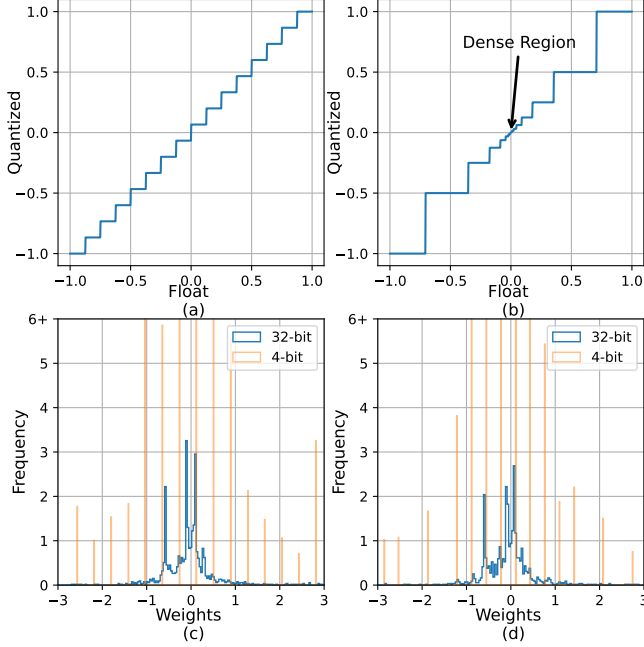


Fig. 2. The quantization levels of (a) uniform and (b) Powers-of-Two quantization. The weights distribution of full-precision 32-bit weights and 4-bit quantized by (c) uniform, (d) PoT.

on CN-Celeb, a large Chinese dataset. The quantized model shows robust performance in the language mismatch SV evaluation.

The paper is organized as follows: Section 2 introduces the details of the quantization methods. The experimental setting and results are given in Sections 3 and 4, respectively. Finally, we give a brief conclusion in Section 5.

2. QUANTIZATION

In a layer with trainable weights, e.g., convolutional layer (CNN) or fully-connected layer (FC), the weights are represented as $\mathcal{W} \in \mathbb{R}$ in continuous values. The quantization of \mathcal{W} is denoted as

$$\widehat{\mathcal{W}} = \Gamma(\lfloor \mathcal{W}, \alpha \rfloor)_{q(\alpha, b)} \quad (1)$$

\mathcal{W} is normalized by its mean and stand deviation, so that it can be represented by a symmetric range. They are clipped into a range of $[-\alpha, \alpha]$ by a function denoted as $\lfloor \cdot, \alpha \rfloor$, where $\alpha (\geq 0)$ is a learnable parameter and will be discussed later. $\Gamma(\cdot)_{q(\alpha, b)}$ represents a projection function, which maps the continuous values into a set of discrete values $\mathbf{q} = [\pm q_1, \pm q_2, \dots, \pm q_{\frac{n}{2}}]$. n is the number of quantization levels, given by 2^b . b is the pre-defined bitwidth, and a larger bitwidth gives a more precise discrete representation of the weights. The design of the quantization level is critical for the quantized models' performance. Uniform and Powers-of-Two quantization are two widely used methods.

2.1. Uniform Quantization

The quantization levels of uniform quantization are represented as

$$\mathbf{q}(\alpha, b) = [0, \frac{\pm 1}{2^{b-1}-1}, \frac{\pm 2}{2^{b-1}-1}, \dots, \pm 1] \times \alpha \quad (2)$$

Uniform quantization generates the discrete values \mathbf{q} evenly along $[-1, 1]$, as illustrated in Fig. 2(a). The length of each quantization level is constant, i.e. $\frac{1}{2^{b-1}-1}$. A smaller length gives a greater ability to distinguish different values, and we refer to this ability as the resolution in this paper. However, the distribution of weights is usually non-uniform [12]. A layer's weight distribution from a trained model is plotted by the blue curve in Fig. 2(c). Several spikes are observed in the distribution. More weights concentrate around the center, and fewer weights lie around the borders. The orange line in Fig. 2(c) shows the uniform quantization level with constant resolution in all regions. The minor numerical differences between weights are erased if they lie in the same quantization level. Thus a large part of the weights around the center will be assigned to an identical value, which degrades the model performance dramatically.

2.2. Powers-of-Two Quantization

The quantization levels of Powers-of-Two (PoT) quantization are represented as

$$\mathbf{q}(\alpha, b) = [0, \pm 2^{-2^{b-1}+1}, \pm 2^{-2^{b-1}+2}, \dots, \pm 1] \times \alpha \quad (3)$$

Different from uniform quantization, PoT provides a non-identical resolution discrete levels, as shown in Fig. 2(b). The quantization levels around the center are denser, which gives a high resolution to represent the weights, as shown by the orange lines in Fig. 2(d). Lower resolutions are proposed near the border. If only a few weights lie around the border, as in Fig. 2(d), the quantization error will not be affected by the low resolutions a lot. Note that the PoT quantizer can be represented as a uniform quantizer in bit-operation form, which is still hardware-friendly.

2.3. Parameter Update

The quantization error ($\|\mathcal{W} - \widehat{\mathcal{W}}\|^2$) is affected by the value of clip threshold α a lot. A large α covers a wide range of the weights' values, while the quantization levels will distribute sparsely. This decreases the resolutions. The α with a small value gives higher resolutions, while there will be more weights outside $[-\alpha, \alpha]$. The outliers are clipped into a constant value, leading to higher quantization errors. The weight distributions of different layers are not identical, and a static clipping may not be optimal for quantizing \mathcal{W} . Learnable α is proposed by Pact [18], where each layer is assigned with an α , and the α is updated in the model training by backward propagation. $\lfloor \cdot, \alpha \rfloor$ and $\Gamma(\cdot)_{q(\alpha, b)}$ are two discrete operations, where the gradients can not be calculated directly. Following [19], the gradients for α and \mathcal{W} are estimated by Straight-Through Estimator (STE) [25] as

$$\frac{\partial \widehat{\mathcal{W}}}{\partial \alpha} = \begin{cases} \text{sign}(\mathcal{W}) & \text{if } |\mathcal{W}| > \alpha \\ \frac{\widehat{\mathcal{W}}}{\alpha} - \frac{\mathcal{W}}{\alpha} & \text{if } |\mathcal{W}| \leq \alpha \end{cases} \quad (4)$$

$$\frac{\partial \mathcal{L}}{\partial \mathcal{W}} = \frac{\partial \mathcal{L}}{\partial \widehat{\mathcal{W}}} \frac{\partial \widehat{\mathcal{W}}}{\partial \mathcal{W}}, \quad \frac{\partial \widehat{\mathcal{W}}}{\partial \mathcal{W}} = 1 \quad (5)$$

where \mathcal{L} represents the training loss. In each training step, the full-precision \mathcal{W} of a layer is transferred into $\widehat{\mathcal{W}}$, and the $\widehat{\mathcal{W}}$ is used for the computation process, such as convolution or matrix multiplication. Thus the calculation of $\frac{\partial \mathcal{L}}{\partial \mathcal{W}}$ can be conducted as the conventional gradient calculation. After training, the \mathcal{W} is quantized into $\widehat{\mathcal{W}}$ with less bitwidth and saved, which compresses the model size.

3. EXPERIMENTAL SETTINGS

3.1. Embedding extraction models

The speaker embedding extraction models used here are ECAPA-TDNN and ResNet. ECAPA-TDNN is proposed by [9], which involves the structures of TDNN [26]. ResNet [24] has a great ability to capture useful features in computer vision tasks, and it has been adopted in SV successfully [8, 27]. They are two widely used DNN-based models in SV, and many models are developed based on them, e.g., MFA-TDNN [28], fwSE-ResNet34 [10]. The convolution layers used in ECAPA-TDNN and ResNet are 1D and 2D, respectively. The effect of quantization on different structures is investigated in these two classic models. ECAPA-TDNN with 512 and 1024 channels are used, and the ResNet34 with 32 channels is chosen.

3.2. Datasets

The datasets utilized in the experiments are VoxCeleb 1&2 (denoted as Vox.1 & Vox.2) [8, 22, 23]. The development set of Vox.2 is used for training models, which consists of 5,994 speakers. Vox.1 is used to evaluate the model performance. Three test sets are constructed using data from Vox.1 and denoted as Original, Easy, and Hard sets, respectively.

3.3. Training strategy

3.3.1. Pre-train in full precision

The training process is first conducted in full precision, i.e., float32 in PyTorch. The model is trained to classify the speaker identity, and additive angular margin softmax (AAM-softmax) [29] is used as the classification loss. The margin and scale of AAM-softmax are set to be 0.2 and 30. We use Adam optimizer [30] with a weight decay of $2e-5$ to train the model. The learning rate is initialized as 0.001 and decayed by a ratio of 0.1 at the 20th, and 32nd epoch, respectively. The entire training process contains 40 epochs.

In each training step, 128 utterances are randomly sampled from the training set and a 2-second long segment is cropped from each input randomly. The raw waveform of each segment is transformed into 64-dimensional *log* MFbanks (FBanks) for the model input, computed with a window size of 25ms and hop length of 10ms, respectively.

Background sound addition and audio reverberation are utilized for data augmentation in training. Background sounds are randomly selected from MUSAN [31]. The simulated room impulse responses sampled from [32] are utilized for audio reverberation.

3.3.2. Fine-tune for compression

The quantized model is fine-tuned from the previously trained full-precision model for 20 epochs. The learning rate is decayed at the 10th and 16th epoch. The data augmentation is abandoned here. The rest of the training settings are kept the same as in the previous section.

3.4. Evaluation protocol

Each utterance is cropped into 4-second long segments evenly, and the overlap between each two adjacent segments equals one second. The cosine similarity values between the test utterance segments and the enrollment segments are averaged as the final score. Adaptive s-norm (AS-norm) [33] is applied to calibrate the scores.

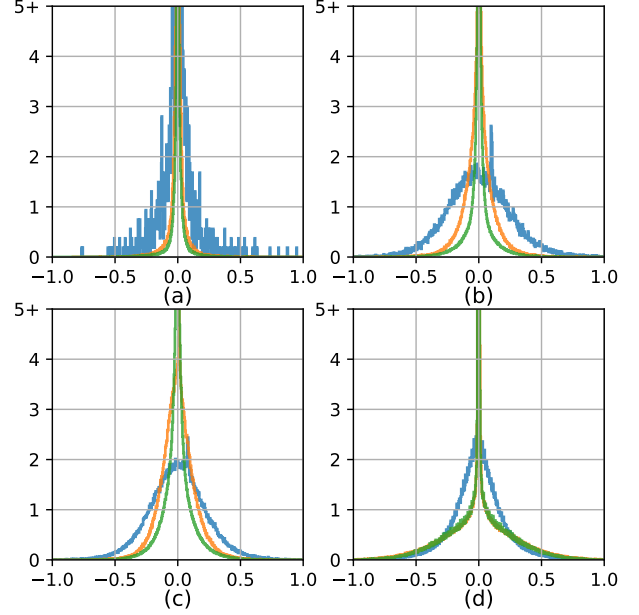


Fig. 3. The weight distributions for (a) the first convolution layer, (b,c) the last convolution layer in the second and third network blocks, and (d) the last FC layer. Orange stands for ECAPA-512, green for ECAPA-1024, and blue for ResNet34. All distributions are normalized. The x-axis represents the value of weights, and the y-axis represents the frequency.

4. RESULTS AND ANALYSIS

Note that the quantization is only applied to the model weights for size compression. The model inputs and activation functions are not quantized. Therefore the processing speed is the same as the unquantized model.

4.1. Learnable quantization

The quantization clip threshold α is updated following Section 2.3 in the model training. The model results on the three test sets of Vox.1 are shown in Table 1. The 8-bit quantization decreases the model size by around 4 times and shows close results on the uniform and PoT quantization. Various effects are observed in different model structures with quantization. The performance decline in ECAPA-TDNN with 512 channels is around 15% in all three test sets. The ECAPA-1024 has the same structure as ECAPA-512 and doubles the channel size, which increases the model complexity and learning ability. ECAPA-1024 outperforms ECAPA-512 in full precision, but gives worse results in the 8-bit quantized models. The performance of ResNet34 is almost not degraded by quantization in all three test sets, showing the robustness of this network structure.

Lower bitwidth is evaluated on ECAPA-512 and ResNet34. Using 4-bit bitwidth, the model size is reduced by around 8 times by the quantization. Different methods show great differences in the results. The 4-bit ECAPA-512 does not converge well in uniform quantization. The quantized model gives 10 times worse EER than the full-precision model. This poor performance can not meet the qualification for real applications. The PoT quantization demonstrates a much better performance for ECAPA-512, but the gap between it and the full-precision model is still tremendous. The decline of ResNet34's performance is significantly less than that of ECAPA-512. The EER on Vox.O is almost the same as its full-precision

Table 1. Performances of the models. Vox.O, Vox.E, Vox.H are short for the Original, Easy and Hard test sets of Vox.1

Model	Parameters (M)	Compression	Bitwidth (bits)	Size (MBytes)	EER(%)		
					Vox.O	Vox.E	Vox.H
ECAPA-TDNN-512	5.95	-	32	23.87	1.07	1.28	2.43
		Uni	8	6.09	1.25	1.47	2.78
		PoT			1.25	1.49	2.82
		Uni	4	3.13	25.28	25.21	26.94
		PoT			6.13	6.04	9.01
ECAPA-TDNN-1024	14.38	-	32	57.61	0.92	1.15	2.28
		Uni	8	14.6	1.31	1.51	2.86
		PoT			1.30	1.52	2.84
ResNet34	6.9	-	32	27.63	1.10	1.15	2.08
		Uni	8	6.96	1.14	1.14	2.06
		PoT			1.13	1.17	2.08
		Uni	4	3.52	1.13	1.21	2.20
		PoT			1.09	1.20	2.14

model, and the results on Vox.E and Vox.H are only decreased by around 5%.

4.2. Distribution analysis

The weight distributions of layers from quantized models are plotted in Fig. 3. Uniform quantization is applied here. The weights are clipped by corresponding learned α and scaled into $[-1, 1]$ for better visualization. It can be observed that the first distribution of ResNet34 is spiky, and other distributions show smooth bell shapes in Fig. 3(b-d). Among the three models, the distributions of ResNet34 are smoother than the other two, and ECAPA-1024 gives the sharpest curves in every shown layer. The distributions from ECAPA-512 become smoother in deeper layers, as shown from Fig. 3(a) to (c). In the last FC layer (Fig. 3(d)), which is connected to the speaker embeddings, both ECAPA-512 and 1024 give a very spiky distribution compared with ResNet34. The peaky distribution of this layer may come from the concatenation operation in the ECAPA structure, which brings peaky distributions like Fig. 3(b) from early layers into the deeper layer. This needs to be studied in future work.

The peak region results in two potential drawbacks. (a) It requires a high resolution to distinguish different values, which increases the difficulty in uniform quantization [19]. This may have led to the failure of the ECAPA in 4-bit uniform quantization. The PoT gives a higher resolution around the center, leading to better results than the uniform quantization in ECAPA-512 using 4-bit. (b) A lower training accuracy is observed on both ECAPA-512 and 1024 than ResNet34. This suggests that their quantized networks' learning ability is decreased with the highly concentrated weights. The smooth weight distribution of ResNet34 may contribute to its great performance in the quantized model and robustness under low-bitwidth quantization.

4.3. Generalization

In addition, to evaluate the generalization ability of the quantized models, they are evaluated on a large Chinese dataset, CN-Celeb [34]. No model fine-tuning is applied on this dataset, and score

Table 2. Performances of the models on CN-Celeb

Model	EER(%)
ECAPA-TDNN-512	1.76
ECAPA-TDNN-512 (PoT,8-bit)	1.68
ResNet34	1.19
ResNet34 (PoT,8-bit)	1.18
ResNet34 (PoT,4-bit)	1.17

normalization is not used. The results are summarized in Table 2. ResNet34 outperforms ECAPA-512 with or without the quantization, which indicates it has a better generalization ability across different languages. Interestingly, the quantized models show superior performance to the full-precision models for both ECAPA-512 and ResNet34. [19] found that quantization may contribute to weight regularization, which may alleviate the overfitting problem of the full-precision model and increase the model generalization in our experiments.

5. CONCLUSIONS AND FUTURE WORK

This paper exploits weight quantization to compress DNN-based SV models. The experiments are carried out on two commonly used SV model structures: ECAPA and ResNet. The ResNet shows robust performance after quantization, while the performance of ECAPA is affected by the quantization methods severely. The quantized models are also evaluated on a Chinese dataset without fine-tuning and show better performance than the full-precision models. This indicates that quantization has an advantage of improving the generalization ability of SV models across different languages. The quantization for model input and activation function will be investigated in the future to speed up the model computation.

6. ACKNOWLEDGEMENTS

The first author is supported by the Hong Kong PhD Fellowship Scheme.

7. REFERENCES

- [1] Joseph P Campbell, “Speaker recognition: A tutorial,” *Proceedings of the IEEE*, vol. 85, no. 9, pp. 1437–1462, 1997.
- [2] Zhizheng Wu, Nicholas Evans, Tomi Kinnunen, et al., “Spoofing and countermeasures for speaker verification: A survey,” *speech communication*, vol. 66, pp. 130–153, 2015.
- [3] Ravika Naika, “An overview of automatic speaker verification system,” *Intelligent Computing and Information and Communication*, pp. 603–610, 2018.
- [4] John HL Hansen and Taufiq Hasan, “Speaker recognition by machines and humans: A tutorial review,” *IEEE Signal processing magazine*, vol. 32, no. 6, pp. 74–99, 2015.
- [5] Douglas A Reynolds and Richard C Rose, “Robust text-independent speaker identification using gaussian mixture speaker models,” *IEEE transactions on speech and audio processing*, vol. 3, no. 1, pp. 72–83, 1995.
- [6] Rong Zheng, Shuwu Zhang, and Bo Xu, “Text-independent speaker identification using gmm-ubm and frame level likelihood normalization,” in *ISCSLP*. IEEE, 2004, pp. 289–292.
- [7] Najim Dehak, Patrick J Kenny, Réda Dehak, Pierre Dumouchel, and Pierre Ouellet, “Front-end factor analysis for speaker verification,” *IEEE Transactions on Audio, Speech, and Language Processing*, vol. 19, no. 4, pp. 788–798, 2010.
- [8] Arsha Nagrani, Joon Son Chung, and Andrew Zisserman, “Voxceleb: A large-scale speaker identification dataset,” *Interspeech*, pp. 2616–2620, 2017.
- [9] Brecht Desplanques, Jenthe Thienpondt, and Kris Demuynck, “Ecapa-tdnn: Emphasized channel attention, propagation and aggregation in tdnn based speaker verification,” *Interspeech*, pp. 3830–3834, 2020.
- [10] Jenthe Thienpondt, Brecht Desplanques, and Kris Demuynck, “Integrating Frequency Translational Invariance in TDNNs and Frequency Positional Information in 2D ResNets to Enhance Speaker Verification,” in *Interspeech*, 2021, pp. 2302–2306.
- [11] Jangho Kim, Simyung Chang, and Nojun Kwak, “PQK: model compression via pruning, quantization, and knowledge distillation,” in *Interspeech*. 2021, pp. 4568–4572, ISCA.
- [12] Song Han, Huizi Mao, and William J Dally, “Deep compression: Compressing deep neural networks with pruning, trained quantization and Huffman coding,” *arXiv preprint arXiv:1510.00149*, 2015.
- [13] Hao Li, Asim Kadav, Igor Durdanovic, et al., “Pruning filters for efficient convnets,” in *ICLR*, 2017.
- [14] Antonio Polino, Razvan Pascanu, and Dan Alistarh, “Model compression via distillation and quantization,” in *ICLR*, 2018.
- [15] Shuchang Zhou, Yuxin Wu, Zekun Ni, et al., “Dorefa-net: Training low bitwidth convolutional neural networks with low bitwidth gradients,” *arXiv preprint arXiv:1606.06160*, 2016.
- [16] Adam Paszke, Sam Gross, Francisco Massa, et al., “Pytorch: An imperative style, high-performance deep learning library,” in *NeurIPS*, 2019, pp. 8024–8035.
- [17] Martín Abadi, Ashish Agarwal, Paul Barham, et al., “TensorFlow: Large-scale machine learning on heterogeneous systems,” 2015, Software available from tensorflow.org.
- [18] Jungwook Choi, Zhuo Wang, Swagath Venkataramani, et al., “Pact: Parameterized clipping activation for quantized neural networks,” *arXiv preprint arXiv:1805.06085*, 2018.
- [19] Yuhang Li, Xin Dong, and Wei Wang, “Additive powers-of-two quantization: An efficient non-uniform discretization for neural networks,” in *ICLR*, 2020.
- [20] Zhaowei Cai, Xiaodong He, Jian Sun, and Nuno Vasconcelos, “Deep learning with low precision by half-wave gaussian quantization,” in *CVPR*, 2017, pp. 5918–5926.
- [21] Aojun Zhou, Anbang Yao, Yiwen Guo, et al., “Incremental network quantization: Towards lossless cnns with low-precision weights,” in *ICLR*, 2017.
- [22] Joon Son Chung, Arsha Nagrani, and Andrew Zisserman, “Voxceleb2: Deep speaker recognition,” *Interspeech*, pp. 1086–1090, 2018.
- [23] Arsha Nagrani, Joon Son Chung, Weidi Xie, and Andrew Zisserman, “Voxceleb: Large-scale speaker verification in the wild,” *Computer Science and Language*, 2019.
- [24] Kaiming He, Xiangyu Zhang, Shaoqing Ren, et al., “Deep residual learning for image recognition,” in *CVPR*, 2016, pp. 770–778.
- [25] Yoshua Bengio, Nicholas Léonard, and Aaron Courville, “Estimating or propagating gradients through stochastic neurons for conditional computation,” *arXiv preprint arXiv:1308.3432*, 2013.
- [26] Vijayaditya Peddinti, Daniel Povey, and Sanjeev Khudanpur, “A time delay neural network architecture for efficient modeling of long temporal contexts,” in *Interspeech*, 2015, pp. 3214–3218.
- [27] Hee Soo Heo, Bong-Jin Lee, Jaesung Huh, et al., “Clova baseline system for the voxceleb speaker recognition challenge 2020,” *arXiv preprint arXiv:2009.14153*, 2020.
- [28] Tianchi Liu, Rohan Kumar Das, Kong Aik Lee, and Haizhou Li, “MFA: TDNN with multi-scale frequency-channel attention for text-independent speaker verification with short utterances,” in *ICASSP*. 2022, pp. 7517–7521, IEEE.
- [29] Jiankang Deng, Jia Guo, Niannan Xue, and Stefanos Zafeiriou, “Arcface: Additive angular margin loss for deep face recognition,” in *CVPR*, 2019, pp. 4690–4699.
- [30] Diederik P. Kingma and Jimmy Ba, “Adam: A method for stochastic optimization,” in *ICLR*, 2015.
- [31] David Snyder, Guoguo Chen, and Daniel Povey, “Musan: A music, speech, and noise corpus,” *arXiv preprint arXiv:1510.08484*, 2015.
- [32] Tom Ko, Vijayaditya Peddinti, Daniel Povey, et al., “A study on data augmentation of reverberant speech for robust speech recognition,” in *ICASSP*. IEEE, 2017, pp. 5220–5224.
- [33] Pavel Matejka, Ondrej Novotný, Oldrich Plchot, et al., “Analysis of score normalization in multilingual speaker recognition,” in *Interspeech*, 2017, pp. 1567–1571.
- [34] Yue Fan, JW Kang, LT Li, et al., “Cn-celeb: a challenging chinese speaker recognition dataset,” in *ICASSP*. IEEE, 2020, pp. 7604–7608.